Kac model from a dynamical system's point of view

Á. Péntek,[1] Z. Toroczkai,[1] D. H. Mayer,[2] and T. Tél[1]
[1]*Institute for Theoretical Physics, Eötvös University, Puskin utca 5-7, H-1088 Budapest, Hungary*
[2]*Institute for Theoretical Physics, University of Clausthal, Leibnizstrasse 10, D-3392 Clausthal-Zellerfeld, Germany*
(Received 12 July 1993)

The Kac model, a spin chain with exponentially decreasing long-range interaction, is investigated by means of a simple functional representation of the transfer operator. An analogy between the thermodynamics of spin chains and of one-dimensional (1D) chaotic maps allows us to use techniques worked out for generalized Frobenius-Perron equations to extract properties of the spin system, such as free energy and the decay rate of the correlation function. Although the Kac chain does not exhibit a phase transition, we find that the correlation decay shows a nonanalytic behavior at some finite temperature. We are also interested in a generalized version of the Kac model where the interaction still decays exponentially but in an oscillating fashion. This leads to the appearance of complicated patterns in the free energy caused by frustration which is a typical effect for disordered systems. By working out the analogy with 1D chaotic maps in more detail, we show how one can construct maps with the same thermodynamics as the spin chain. The associated maps turn out to be not smoothly differentiable, and their derivatives exhibit fractal properties.

PACS number(s): 64.60.Cn, 05.50.+q, 05.45.+b

I. INTRODUCTION

The thermodynamical formalism of dynamical systems establishes a connection between multifractal-like properties of low-dimensional chaotic processes and the statistical physics of spin chains. The key observation is that codes of length n appearing in the symbolic description of the dynamics can uniquely be mapped onto the microstates of spin chains of length n. The number of different codes needed in the symbolic dynamics corresponds to the number of possible spin orientations. Binary encoding corresponds to Ising type spins.

Based on classical mathematical papers [1–3], this formalism has recently become a common tool for both mathematicians [4–6] and physicists [7–30]. Research has mainly been focused on the determination of the spin chains associated with given chaotic systems. These studies showed [31–38] that apart from a few trivial examples, like, e.g., the tent map, even simple maps lead to systems characterized by rather complicated (long-ranged and multispin) interactions.

Here we follow an approach going in the opposite direction. We select a nontrivial spin system with a relatively simple interaction and ask what the associated one-dimensional map looks like. It will turn out that the map is no longer smooth and its derivative possesses fractal properties. More precisely, there is a class of such maps belonging to the same spin system.

Our working example is the so-called Kac model [39–42], a spin chain with *exponentially decreasing* long-range interaction. The essential parameter is the spatial decay rate λ of the interaction.

An appealing feature of this model is that methods known from the theory of dynamical systems can successfully be applied to computing its *thermal properties*. This is based on a result obtained by Viswanathan and Mayer [43] who showed that the free-energy density $\mathcal{F}(\beta)$ of the Kac model at inverse temperature β can be obtained from the largest eigenvalue of an operator $\mathcal{L}$ acting on smooth functions $g(x)$ defined as

$$\mathcal{L}\, g(x) = \sum_{\sigma=\pm 1} \exp(\beta\sigma x)\, g(\lambda\sigma + \lambda x). \tag{1}$$

This operator, which will be derived in Sec. III, is much easier to handle than the standard transfer matrix that is infinite dimensional in this case. The form of Eq. (1) ensures that the free energy can be obtained by studying the iteration of simple functions, i.e., by solving the eigenvalue equation in an iterative way.

This is the point where an analogy with a branch of the dynamical system's theory can be found. The so-called generalized Frobenius-Perron operator [24–30] has widely been used to characterize scaling properties of one-dimensional maps. For a single humped map $f(x)$ with two inverse branches $F_\epsilon(y)$, $\epsilon = 0, 1$, the operator H is given as

$$H\psi(x) = \sum_{\epsilon=0,1} |\, F'_\epsilon(x)\,|^\beta \psi(F_\epsilon(x)). \tag{2}$$

Here ψ is a function defined on the support of the map $f(x)$, and $-\infty < \beta < \infty$ is a weighting parameter. The free energy $F(\beta)$ of the map f obtained in the spirit of thermodynamical formalism [3,7,9] is connected with the largest eigenvalue of H [25].

Although the complete equivalence of Eqs. (1) and (2) is not obvious at a first glance, their similarity is striking. They both represent a binary structure, and the largest eigenvalues can be obtained by letting the operators repeatedly act on some function and by extracting the growth rate of the iteration.

We used the numerical techniques worked out for generalized Frobenius-Perron equations to solve for the leading and for a few next to leading eigenvalues of Eq. (1). It turns out that the procedure is much faster than the application of the transfer-matrix method and allows thus for studying the temperature dependence in a broad range.

The finding of a one-dimensional map whose free energy $F(\beta)$ is the same, apart from an energy constant, as the free energy $\mathcal{F}(\beta)$ of the Kac model, means that Eqs. (1) and (2) can really be equivalent. This will be seen to hold, however, if the associated map $f(x)$ is not smoothly differentiable.

In order to see the results in a broader context, we also allow for generalizations of the Kac model obtained by introducing a homogeneous magnetic field and by letting the interaction parameter λ of the model to be complex. The latter corresponds to an interaction which decays in an oscillating fashion whose wavelength is governed by the imaginary part of λ.

The paper is organized as follows. In Sec. II the Kac model and its generalizations are introduced. Next (Sec. III), a brief summary of the transfer operator method is given, and the application of this method to the Kac model leads to the operator $\mathcal{L}$ defined by Eq. (1). The properties of the free energy and the associated eigenfunction are discussed in Sec. IV. Introducing an external field leads to symmetry breaking in the eigenfunction, while a complex extension of the coupling constant results in the appearance of interesting patterns in the free energy. Methods for determining the second and third eigenvalues are presented in Secs. V and VI. We show that between the moduli of these eigenvalues a level crossing occurs which implies the existence of two β regimes with qualitatively different decay properties in the correlation function or in the finite size corrections of the spin system. Finally, the map associated with the Kac model is constructed in Sec. VII and the relevance of the energy constant for the form of the map is studied in Sec. VIII. Some concluding remarks are given in Sec. IX.

II. THE KAC MODEL

The Kac model [39–42] is a chain of two-state spins of Ising type characterized by an exponentially decreasing interaction. Its Hamiltonian in the presence of a constant magnetic field h is given by

$$\mathcal{H} = -\frac{J}{2}\sum_{i\neq j}\sigma_i\sigma_j\lambda^{|j-i|} - h\sum_i \sigma_i, \tag{3}$$

where J is a coupling constant and $0 < \lambda < 1$ describes the decay of the interaction. The lattice constant will be taken to be unity. Historically, the Kac model was introduced as a nontrivial example for demonstrating the existence of a second order phase transition in a system with long-range interaction. The limit $\lambda \to 1$, $J \to 0$ leads in a nontrivial way to the degeneration of the highest eigenvalues and a mean field behavior which has extensively been studied [40,42]. Here we shall be interested in cases where $\lambda < 1$ and, consequently, where *no phase transition* takes place because of the exponential decay of the interaction. Thus we know that the free energy is analytic, but cannot exclude the existence of nonanalytic behavior in the second eigenvalue. Such nonanalyticity has been found, for example, in the surface correlation function for the two-dimensional Ising model in the presence of enhanced surface couplings [44]. One of our aims will be, therefore, to compute the free energy and some next-to-leading eigenvalues in a broad range of the inverse temperature which, to our knowledge, has not been discussed in the literature.

It is interesting to note that the Kac chain also appears in the theory of Frenkel-Kontorova-like models of amorphous solids. Associating an appropriate symbolic encoding $\{\sigma_i\}$ to equilibrium configurations of the one-dimensional Frenkel-Kontorova chain with piecewise parabolic interactions, one finds that the total energy of configuration $\{\sigma_i\}$ is given, up to an additive constant, by Eq. (3) [45]. In cases when all binary configurations are allowed in the disordered system, like, e.g., in a parameter range of the Reichert-Schilling model [46], there is a one-to-one correspondence between the Kac and the Frenkel-Kontorova models.

We shall also be interested in a version of the Kac model which contains a complex interaction parameter λ but is defined by the real Hamiltonian

$$\mathcal{H} = -\frac{J}{4}\sum_{i\neq j}\sigma_i\sigma_j(\lambda^{|j-i|} + \lambda^{*|j-i|}) - h\sum_i \sigma_i. \tag{4}$$

Here we assume that $|\lambda| < 1$. The physical relevance of this case can be seen by introducing φ as the phase of λ and noting that the interaction between two sites of distance x decays exponentially but now with an *oscillating amplitude* $|\lambda|^x \cos\varphi x$. This oscillation mimics the effect of the indirect exchange interaction between spins which is mediated by electrons and is known to lead to RKKY type interaction in realistic spin models [48] where the decay is, however, algebraic. The extended model also enables us to study an effect which is typical for disordered systems, the *frustration* [49]. This means that there exist spin triples which have no configuration that satisfies all the bonds.

III. THE TRANSFER OPERATOR

In this section we briefly summarize the transfer operator approach [3,50] which can be viewed as an extension of the transfer-matrix method [51,52] to systems with infinite range interactions. Let us consider a semi-infinite chain of spins characterized by the configuration $\underline{\xi} = (\xi_1, \xi_2, \xi_3, \ldots, \xi_i, \ldots)$ where i labels the site of spin ξ_i. We assume that the spins can take two values, -1 or 1, only. Now let us add a new spin σ to site 0. The key observation is that the average value of any smooth physical quantity $g(\sigma, \underline{\xi})$, like, e.g., the magnetization, at inverse temperature β and at fixed configuration $\underline{\xi}$ can be computed by the use of an operator $\mathcal{L}$ defined by

$$\mathcal{L}g(\underline{\xi}) = \sum_{\sigma=\pm 1} \exp\left[-\beta W(\sigma,\underline{\xi})\right] g(\sigma,\underline{\xi}), \tag{5}$$

where $W(\sigma,\underline{\xi})$ denotes the interaction energy of spin σ with the semi-infinite chain at configuration $\underline{\xi}$. Note that Eq. (5) describes nothing but the averaging process over the new microstates appeared by adding the spin σ as illustrated by Fig. 1.

The importance of transfer operator $\mathcal{L}$ lies in its repeated applicability when adding further spins to the system at its left end. After $n \gg 1$ iterations, the original configuration $\underline{\xi}$ becomes gradually irrelevant and as $n \to \infty$ the procedure describes properties of the spin system valid in the thermodynamic limit. In particular, $\mathcal{L}^n g$ is expected to grow as $\exp\left[-\beta\mathcal{F}(\beta)n\right]$ where $\mathcal{F}(\beta)$ is the free energy density of the system. On the other hand, $\exp\left[-\beta\mathcal{F}(\beta)n\right]$ should grow as the nth power of the largest eigenvalue $\lambda_1(\beta)$ of the transfer operator in the class of smooth functions. Consequently, $\lambda_1(\beta)$ is positive and we have

$$\lambda_1(\beta) = e^{-\beta\mathcal{F}(\beta)} \tag{6}$$

(for a rigorous proof see [50]). More precisely, one can write

$$\frac{\mathcal{L}^n g}{\lambda_1^n(\beta)} \to g_1, \tag{7}$$

where g_1 is an eigenfunction belonging to the first eigenvalue of the transfer operator and the formula is valid for any smooth g in a broad class of functions (for details see the discussion in Sec. V). Thus one can always use, e.g., the identity function $g(\underline{\xi}) \equiv 1$ when computing the largest eigenvalue and the corresponding eigenfunction. Since the operator $\mathcal{L}$ is positive [50], it also follows that the largest eigenvalue $\lambda_1(\beta)$ is separated from the rest of the spectrum: $\lambda_1(\beta) > \lambda_2(\beta) \geq \lambda_3(\beta) \ldots$. Consequently, the convergence is exponentially fast.

In the case of the Ising chain with nearest-neighbor interaction, one can immediately rewrite Eq. (5) in a matrix form and the matrix representation of $\mathcal{L}$ turns out then to be the transfer matrix [51]. The real advantage of the transfer operator is that it provides a method applicable to cases with long-range interactions when the classical transfer matrix would be of $\infty \times \infty$ type and, therefore, difficult to handle. It is of particular importance that the action of the operator can then, in certain cases, be transformed into a simple functional recursion [50] the numerical solution of which is much easier than that of a matrix representation of Eq. (5) obtained by truncating the interactions at some finite distance.

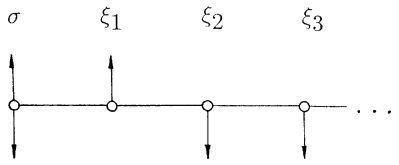

FIG. 1. Schematic diagram illustrating the action of the transfer operator when averaging out the spin variable σ at a fixed configuration $\underline{\xi}$.

The transfer operator for the Kac model follows from Eqs. (3) and (5) to be

$$\mathcal{L}g(\underline{\xi}) = \sum_{\sigma=\pm 1} \exp\left[\beta\sigma\left(J\sum_{i=1}^{\infty}\xi_i\lambda^i + h\right)\right] g(\sigma,\underline{\xi}). \tag{8}$$

The key point is that $\mathcal{L}g(\underline{\xi})$ depends on the combination

$$x = \sum_{i=1}^{\infty}\xi_i\lambda^i \tag{9}$$

only. Due to the infinity of all possible spin configurations, the quantity x is a variable taking real values between $-\lambda/(1-\lambda)$ and $\lambda/(1-\lambda)$. By considering the physical quantity g at a configuration $\underline{\xi}$ to be some function of x, i.e., $g(\underline{\xi}) = g(x)$, the same physical quantity $g(\sigma,\underline{\xi})$ of the chain supplemented by spin σ can be written as

$$g(\sigma,\underline{\xi}) = g(\sigma\lambda + \xi_1\lambda^2 + \xi_2\lambda^3 + \cdots) = g(\lambda\sigma + \lambda x). \tag{10}$$

All the real numbers x which correspond to a given spin configuration $\underline{\xi}$ are mapped onto $\sigma\lambda + \lambda x$, corresponding to another configuration $(\sigma,\underline{\xi})$. By extending the variable x on the whole real axis, the nonphysical x values, which do not correspond to a configuration $\underline{\xi}$ or are larger in modulus than $\lambda/(1-\lambda)$, are mapped onto another nonphysical value or a value larger in modulus than $\lambda/(1-\lambda)$ again. Therefore, in what follows, we consider x as a *continuous* real variable without any restriction, because this assumption does not affect the computation of the relevant physical quantities. This means that g can be chosen to be in the space of single-variable real functions since the action of the operator does not lead out of this space. Consequently, the transfer operator can be represented by the form

$$\mathcal{L}g(x) = \sum_{\sigma=\pm 1} \exp\left[\beta\sigma(Jx + h)\right] g(\lambda\sigma + \lambda x). \tag{11}$$

This representation of the transfer operator was first obtained by Viswanathan and Mayer [43,50]. These authors also showed that their form was equivalent to the integral operator derived by Kac [39] from which it also follows that the spectrum of $\mathcal{L}$ is real and discrete. That the spectrum of the two transfer operators are the same was shown by Moritz in his diploma thesis [53].

For the complex version, see Eq. (4), the transfer operator

$$\mathcal{L}g(\underline{\xi}) = \sum_{\sigma=\pm 1} \exp\left[\beta\sigma\left(\frac{J}{2}\sum_{i=1}^{\infty}\xi_i(\lambda^i + \lambda^{*i}) + h\right)\right] g(\sigma,\underline{\xi}) \tag{12}$$

is a function of both variables

$$z_1 = \sum_{i=1}^{\infty}\xi_i\lambda^i \quad \text{and} \quad z_2 = \sum_{i=1}^{\infty}\xi_i\lambda^{*i}. \tag{13}$$

When writing $g(\underline{\xi}_1,\xi_2,\ldots) = g(z_1,z_2)$ one immediately

finds that $g(\sigma,\xi_1,\xi_2,\ldots)$ is of the form $g(\lambda\sigma+\lambda z_1,\lambda^*\sigma+\lambda^* z_2)$, i.e., g can now be represented as a function holomorphic in two complex variables z_1 and z_2. The corresponding transfer operator then reads as

$$\mathcal{L}g(z_1,z_2)=\sum_{\sigma=\pm1}\exp\left[\beta\sigma\left(\frac{J}{2}(z_1+z_2)+h\right)\right]\times g(\lambda\sigma+\lambda z_1,\lambda^*\sigma+\lambda^* z_2). \tag{14}$$

This equation is a straightforward bivariate extension of Eq. (11).

Proceeding as in [50] one shows that $\mathcal{L}$ is of traceclass when acting in the above-mentioned space of functions g, holomorphic in z_1 and z_2 in the disks $\mid z_i \mid < R$ if $R > \mid\lambda\mid/(1-\mid\lambda\mid)$. Arguments similar to the ones given in [50] show that $\mathcal{L}$ has a leading positive eigenvalue strictly larger in modulus than the remaining eigenvalues.

Note that in both operators (11) and (14) the coupling constant J appears only as a coefficient of β. Consequently, by an appropriate rescaling of the inverse temperature and the magnetic field we can always choose

$$J=1 \tag{15}$$

provided the coupling is of ferromagnetic type, i.e., $J>0$. Antiferromagnetic cases can then be obtained by applying the transformation $\beta\to-\beta, h\to-h$.

The determination of the leading eigenvalues and eigenfunctions of operators (11) and (14) is based on their repeated application to some test functions which is carried out numerically by repetitive function calls just like in the case of the generalized Frobenius-Perron equations.

IV. THE FREE ENERGY

The free energy $\mathcal{F}(\beta)$ of the Kac model at inverse temperature β has been computed from the relation

$$\mathcal{L}^n g\sim e^{-\beta\mathcal{F}(\beta)n} \tag{16}$$

valid for $n\gg1$ or, equivalently, from

$$\beta\mathcal{F}(\beta)\cong\ln\frac{\mathcal{L}^n g}{\mathcal{L}^{n-1}g}. \tag{17}$$

As initial functions we chose, if not stated otherwise, $g(x)\equiv1$ in the real case and $g(z_1,z_2)\equiv1$ in the complex case. The error of the computation has been estimated by evaluating

$$\delta(\beta)=\ln\frac{(\mathcal{L}^{n+1}g)(\mathcal{L}^{n-1}g)}{(\mathcal{L}^n g)^2}. \tag{18}$$

Because of the exponentially fast convergence in n, an error of 10^{-4} can be reached at a number of $n=10$ in a broad range of β values. It is worth comparing the efficiency of this approach with that of the classical transfer matrix method. By truncating the range of interaction at a size of $m=7$, the CPU time needed for the computation of the largest eigenvalue of the $2^m\times2^m$ transfer matrix, by letting it act on an arbitrary vector and extracting the growth rate, was about two orders of magnitude longer (and less accurate) than by means of the functional iteration described above.

A. The real case

Figure 2 shows the free energy obtained in this way at different values of the interaction parameter λ and of the magnetic field, respectively. A smooth dependence on these quantities has been found.

The difference between cases with and without magnetic field becomes more drastic when taking into consideration the corresponding eigenfunctions, too. In the absence of any external field the eigenfunction is even but this symmetry is lost by switching on the field. The asymmetry is the stronger the larger is the magnetic field.

By substituting the form

$$g(x)\equiv\exp(\alpha\mid x\mid) \tag{19}$$

into the eigenvalue equation for $\mid x\mid\gg1$, one easily finds that

$$\alpha=\frac{\mid\beta\mid}{1-\lambda} \tag{20}$$

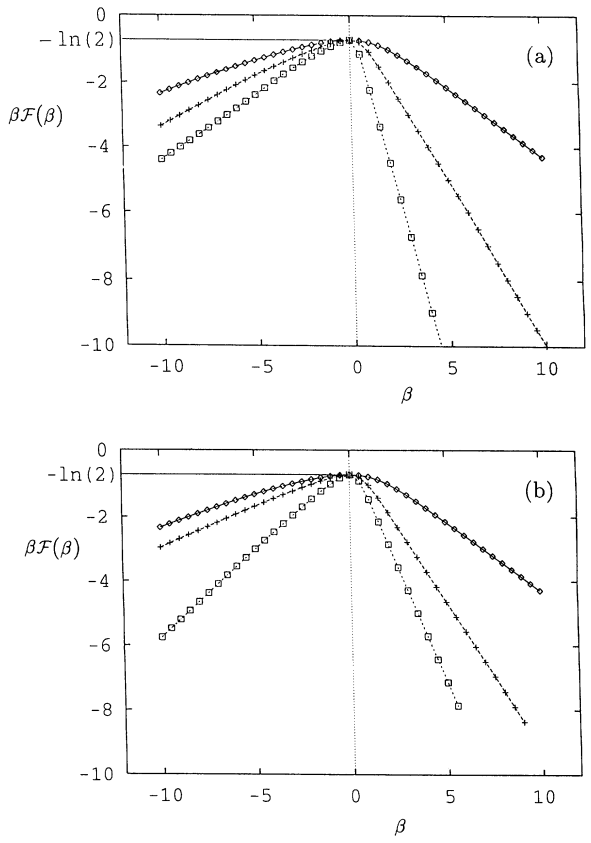

FIG. 2. Free energy of the Kac chain at different values of the interaction parameter and of the magnetic field (a) λ=0.3 ($\diamond$), 0.5 (+), 0.7 ($\square$) at $h=0$; (b) h =0 ($\diamond$), 0.5 (+), 1.0 ($\square$) at $\lambda=0.3$. Results were obtained by iterating the transfer operator (11) $n=10$ times and by using relation (17). The maximal error in the range $\mid\beta\mid<5$ is 10^{-4} and grows up to 10^{-2} around $\mid\beta\mid\approx10$.

for any value of the magnetic field. This means that the eigenfunctions belonging to any finite eigenvalue are exponentially increasing for large positive or negative values of x, unless the temperature is infinite.

In view of this observation, it is worth plotting the eigenfunction $g_1(x)$ after dividing it with $\cosh(\alpha x)$ which makes the graph bounded. Figure 3 exhibits the first eigenfunction with this normalization at different values of the magnetic field. The convergence toward the limiting value with n is also shown. Note the strong asymmetry in both the function's form and the convergence rate in the presence of the field.

B. The complex case

In the case of complex interaction parameter λ an interesting new phenomenon shows up. The free energy does not exhibit a monotonic behavior by increasing the imaginary part $\lambda_{\rm im}$ at a fixed real part $\lambda_{\rm re}$. Another appearance of the same fact is an oscillating behavior found in the free energy when plotted as a function of the phase φ at $\mid \lambda \mid$ fixed. This can be understood by recalling that the interaction energy between two spins σ_i and σ_{i+k} is proportional to $\mid \lambda \mid^k \cos(k\varphi)$. Consequently, the total interaction energy appears as a weighted sum of terms of the type $\mid \lambda \mid^k \cos(k\varphi)$, i.e., it is of a kind of Fourier series. As a function of φ, it shows therefore interference patterns which also survive in the free energy taken at finite temperatures (see Fig. 4). The strength of the interference depends on λ. In particular, when $\mid \lambda \mid \ll 1$ the nearest-neighbor interactions dominate and the system is close to an Ising chain with coupling constant $\mid \lambda \mid \cos(\varphi)$. The free energy is then well approximated by that of the Ising model, i.e., $\beta\mathcal{F}(\beta) = -\ln\cosh[\beta \mid \lambda \mid \cos(\varphi)]$. This π periodicity can clearly be seen in Fig. 4(a). Note that the maximum at $\varphi = \pi/2$ corresponds to a configuration where the interaction energy exactly vanishes at the first neighbors. This is a very loosely bounded state and possesses, therefore, a free energy value lying closest to that of the free spin chain $(-\ln 2)$. By increasing $\mid \lambda \mid$, longer and longer interactions play a dominant role and this leads to complicated φ dependences [see, e.g., Fig. 4(b)].

The effect of frustration can occur at any complex value of λ if there exist spin triples with at least one bond which is not satisfied energetically, i.e., the spin pair belonging to this bond is not in its lowest energy

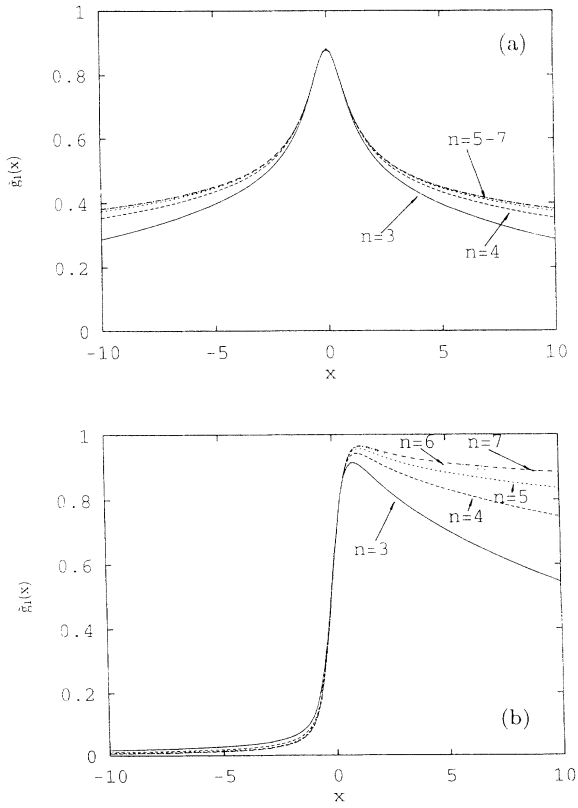

FIG. 3. The eigenfunctions g_1 of the transfer operator corresponding to the largest eigenvalue: (a) $h = 0$, the eigenfunction is even; (b) $h = 0.1$, the symmetry of the eigenfunctions is destroyed by the magnetic field. Notice in each figure the very fast convergence (the eigenfunctions are plotted for $n = 3, 4, \ldots, 7$). The eigenfunctions were computed at $\lambda = 0.3$ and $\beta = 1.2$ via Eq. (7). The diverging asymptotic behavior has been removed by plotting $\tilde{g}_1 = g_1/\cosh(\alpha x)$.

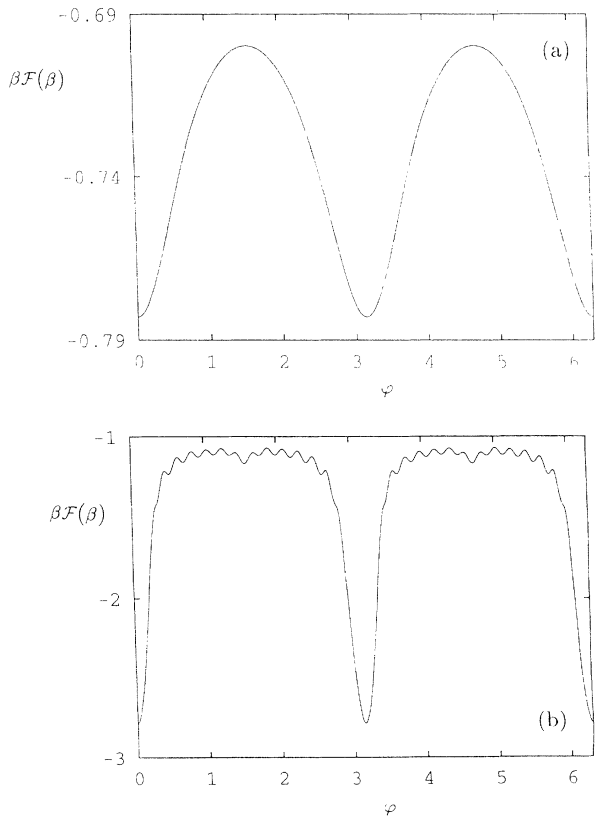

FIG. 4. The free energy at $\beta = 1.2$ for $h = 0$ as function of the phase $0 \leq \varphi \leq 2\pi$ of λ. Results are obtained after $n = 14$ iterations of the transfer operator. The maximal error is 10^{-2}. (a) $\mid \lambda \mid = 0.3$. The two maxima belong to the case when the interaction energy vanishes at nearest neighbors at $\varphi = \pi/2$ and $3\pi/2$. (b) $\mid \lambda \mid = 0.7$. The small wavelength oscillations are interference effects.

state. A sufficient condition for frustration is, therefore, that the nearest-neighbor interaction is negative, $\cos(\varphi) > 0$ but the next-nearest-neighbor interaction is positive, $\cos(2\varphi) < 0$, or if both kind of bonds have positive signs: $\cos(\varphi) < 0$ and $\cos(2\varphi) < 0$. This is fulfilled in the range $\pi/4 \leq \varphi \leq 3\pi/4$. Thus we see that frustration is accompanied with a loose bond and a relatively large value of the free energy.

V. HIGHER EIGENVALUES

When studying higher eigenvalues of the transfer operator we restrict our attention to the real case without any magnetic field since similar effects are expected to show up in more complicated cases, too.

Let us first observe that because of the symmetry of the transfer operator, the image $\mathcal{L}g(x)$ of $g(x)$ is an even (odd) function if $g(x)$ was even (odd). In other words, the class of even (odd) functions forms an invariant subspace of the function space. The eigenfunction belonging to the first eigenvalue is even [50] as also illustrated by Fig. 3(a). It can be obtained by applying $\mathcal{L}$ several times to any $g(x)$ which is not antisymmetric. Iterations then lead into the class of even functions. An application of $\mathcal{L}$ to odd functions, however, will stay within this class, and the quantity ρ_2 obtained as

$$\rho_2(\beta) = \frac{\mathcal{L}^{n+1}g_0(x)}{\mathcal{L}^n g_0(x)}, \qquad n \gg 1 \tag{21}$$

will be different from the largest eigenvalue $\lambda_1(\beta)$. We shall call ρ_2 the *iteratively obtained* largest eigenvalue in the space of odd functions.

Our finding is that $\rho_2(\beta)$ is positive and monotonically increasing with β in a range $\beta > \beta_c$. Below a critical value $\beta_c < 0$, however, $\rho_2(\beta)$ *becomes negative* and at β_c a jump occurs (see Fig. 5). This behavior seems to be associated with a drastic change in the form of the eigenfunctions g_2 belonging to ρ_2. For $\beta > \beta_c$ g_2 is a monotonic increasing function but develops several nodes below β_c.

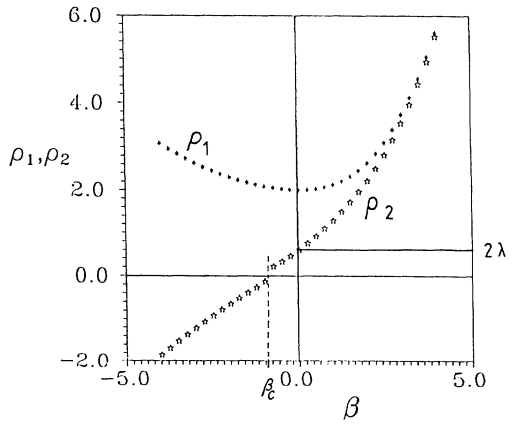

FIG. 5. The first iteratively obtained eigenvalues $\rho_1 \equiv \lambda_1$ and ρ_2 belonging to the class of even and odd eigenfunctions, respectively, at $\lambda = 0.3$ and $h = 0$. Notice the jump in ρ_2 at $\beta_c \simeq -1$. The number of iterations used was $n = 10$. The maximal error is 10^{-2}. It is easy to check that $\rho_2(\beta = 0) = 2\lambda$.

An approximate critical value $\beta_c^{(0)}$ easily follows from a simple argument. By taking $g_0(x) \equiv x$, the first image function is

$$g_1(x) = 2\lambda[\sinh(\beta x) + x\cosh(\beta x)]. \tag{22}$$

Consequently, g_1 possesses two nontrivial nodes

$$x^* = -\tanh(\beta x^*) \tag{23}$$

provided $\beta < \beta_c^{(0)}$ where $\beta_c^{(0)} = -1$. Note that this is exactly the same argument one uses in the mean-field theory of ferromagnets [47].

The condition found above for the development of nodes in the eigenfunction is necessary but not sufficient. It can happen that $\mathcal{L}g_0(x)$ does not have yet any node but $\mathcal{L}^2 g_0(x)$ does. The true critical value β_c belongs to the case when $\mathcal{L}^{n\to\infty}g_0(x)$ first develops nodes. In fact, $\beta_c^{(0)} = -1$ turns out to be just a zeroth order result valid for $\lambda \to 0$. The true critical value has numerically been found to be larger than $\beta_c^{(0)}$.

One can easily convince himself that for $\beta < \beta_c$ an *infinity of nodes* evolves and they asymptotically follow a geometric series with quotient $1/\lambda$ (see Fig. 6 and Appendix A). By taking into account this rule and the general asymptotic form of any eigenfunction found in Eq. (19), we conclude that $g_2(x)$ must behave for large values of $|x|$ as

$$g_2(x) \sim \sinh(\alpha x)\, G\left(\frac{2\pi}{\ln 1/\lambda}\ln|x| + \omega\right), \tag{24}$$

where α is given by Eq. (20), G is a 2π-periodic function and ω is an arbitrary constant.

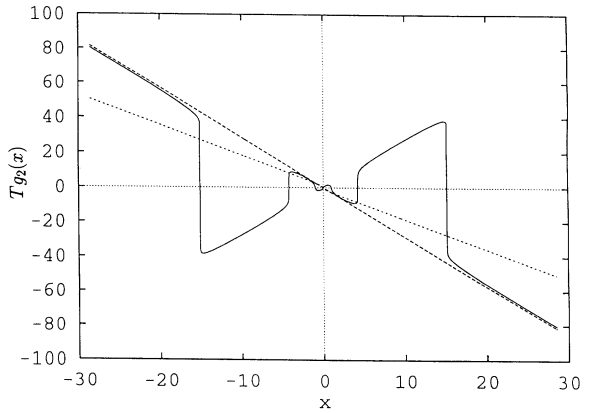

FIG. 6. The eigenfunction g_2 below the critical point. Here $\beta = -2 < \beta_c$, $\lambda = 0.3$, and $h = 0$ is taken. In order to visualize the structure of g_2, we plotted a transformed version $Tg_2(x) = \mathrm{sgn}[g_2(x)]\ln(1+|g_2(x)|)$ (full line). The heavy dashed line has a slope $\beta/(1-\lambda)$ in agreement with the form given by Eq. (24). For comparison, the eigenfunction belonging to ρ_2 above β_c ($\beta = 1.2 > \beta_c$) is also shown (dashed line) and is difficult to distinguish from a straight line in this representation.

VI. LEVEL CROSSINGS

As an explanation of the jump in the iteratively obtained second largest eigenvalue ρ_2 at β_c, we first note that the iteration process $\mathcal{L}^n g_0(x)$ is always dominated by that eigenvalue which is largest in *modulus*. Thus ρ_2 in Eq. (21) has the property $|\rho_2(\beta)| > |\lambda_i(\beta)|$ for any eigenvalue $\lambda_i(\beta)$ in the class of antisymmetric functions. We also note that this property does not exclude the possibility that ρ_2 is negative.

Numerically, Eq. (21) converges very fast except in the neighborhood of β_c where the convergence becomes bad; therefore, relation (21) cannot be used in practice to find ρ_2 there. Usually, when iterating linear operators, this effect is due to a crossing of two eigenvalue branches. To see if this is the case here, we also computed $\rho_4(\beta)$, the second largest iteratively obtained eigenvalue in the space of odd functions which is defined via the asymptotic form

$$\mathcal{L}^n g_0(x) = \rho_2^n(\beta)A(x) + \rho_4^n(\beta)B(x) + \cdots, \quad n \gg 1. \tag{25}$$

The coefficients $A(x), B(x)$ are n-independent quantities. Eigenvalue ρ_4 then follows from the relation

$$\rho_4(\beta) = \frac{\mathcal{L}^{n+1}g_0(x) - \rho_2(\beta)\mathcal{L}^n g_0(x)}{\mathcal{L}^n g_0(x) - \rho_2(\beta)\mathcal{L}^{n-1}g_0(x)}. \tag{26}$$

This formula is valid apart from a neighborhood of β_c where $\rho_2(\beta)$ and $\rho_4(\beta)$ cannot be found by means of Eqs. (21) and (26). In this regime we used a different method to compute ρ_2 and ρ_4 which is described in Appendix B.

We have found that ρ_4 in the range $\beta < \beta_c$ is the analytical continuation of ρ_2 from $\beta > \beta_c$ and, analogously, ρ_4 in the range $\beta > \beta_c$ is the analytical continuation of ρ_2 from $\beta < \beta_c$. Consequently, we can also say that there are two eigenvalues $\lambda_2(\beta)$ and $\lambda_4(\beta)$ which are *analytic expressions* of β with the following properties:

$$\lambda_2(\beta) = \begin{cases} \rho_2(\beta) & \text{for } \beta \geq \beta_c \\ \rho_4(\beta) & \text{for } \beta < \beta_c, \end{cases} \tag{27}$$

$$\lambda_4(\beta) = \begin{cases} \rho_4(\beta) & \text{for } \beta \geq \beta_c \\ \rho_2(\beta) & \text{for } \beta < \beta_c, \end{cases} \tag{28}$$

and at $\beta = \beta_c$ $\lambda_2(\beta) = -\lambda_4(\beta)$. These functions are plotted in Fig. 7 for $\lambda = 0.3$. This is supported very well by the fact that the form of $\lambda_2(\beta)$ can be analytically given for $\lambda = 1/2$. One can easily check that the second largest eigenvalue is then given by

$$\lambda_2(\beta) = e^{\beta} \tag{29}$$

and the corresponding eigenfunction is $\sinh(2\beta x)$.

Therefore, the nonanalytic behavior of $\rho_2(\beta)$ at β_c is explained as a *level crossing* between the moduli of the analytic curves λ_2 and λ_4; see Fig. 7. It is to be noted that $\lambda_2(\beta)$ defined above is strictly positive; for all other eigenvalues $\lambda_2 > \lambda_i$ for any temperature. The spectrum is not degenerate, i.e., the curves λ_i do not cross each other. Level crossing occurs in the absolute values of

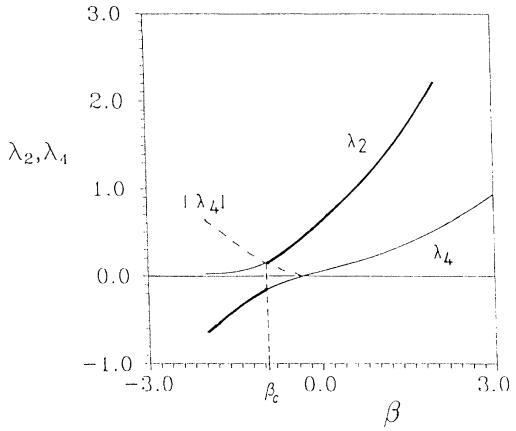

FIG. 7. The eigenvalues λ_2, λ_4 at $\lambda = 0.3$, $h = 0$. The level crossing of the curves λ_2 and $|\lambda_4|$ (dashed line) causes the critical behavior at $\beta_c = -0.947$. The heavy line is the largest iteratively obtainable eigenvalue belonging to the odd eigenfunctions (ρ_2). Around the critical point the eigenvalues were computed by means of the method described in Appendix B. The eigenfunctions belonging to λ_2 and λ_4 are of similar type as the ones belonging to the second largest iteratively obtained eigenvalue for $\beta > \beta_c$ and $\beta < \beta_c$, respectively (see Fig. 6).

the eigenvalues. Thus $\lambda_2(\beta)$ is really the second largest eigenvalue of $\mathcal{L}$ but it is *not greater* than the modulus of all other eigenvalues in the whole β region.

In a different vein, we started iterations of the operator $\mathcal{L}$ with functions which are neither symmetric nor antisymmetric. We observed that the quantity $\mathcal{L}^{n+1}g_0(x)/\mathcal{L}^n g_0(x)$ in this case goes to the first eigenvalue $\lambda_1(\beta) \equiv \rho_1(\beta)$ found when starting from the class of symmetric functions, and the convergence to λ_1 is governed by $\rho_2(\beta)$:

$$\mathcal{L}^n g_0(x) = \rho_1^n(\beta)D(x) + \rho_2^n(\beta)E(x) + \cdots, \quad n \gg 1. \tag{30}$$

$g_0(x)$ is here neither symmetric nor antisymmetric.

We have also checked that the second highest iteratively obtained eigenvalue ρ_2 of the operator $\mathcal{L}$ is the same as the one computed from the transfer matrix of the Kac model, although this procedure is less accurate.

When applying the transfer matrix to a spin system with finite range interactions, the ratio of the next-to-leading and leading eigenvalue determines the decay rate of the *correlation function* [47]. The same quantity simultaneously controls how the *finite size corrections* vanish when the thermodynamic limit is taken [54]. Repeated applications of the transfer matrix corresponds to an iterative solution of the transfer operator problem. Therefore, it is the *iteratively obtained* second largest eigenvalue ρ_2 that is relevant from the point of view of the aforementioned quantities in systems with long-range interactions. In other words, the correlation function between two spins σ_k and σ_{k+r} of the infinite chain can be written as $\sum_{i=2}^{\infty} c_i[\lambda_i(\beta)/\lambda_1(\beta)]^r$ where the coefficients c_i are constant [39]. This is an analytic function for finite

r in both r and β. In the limit $r \to \infty$ the decay is dominated by the eigenvalue *largest in modulus* and goes as $[\rho_2(\beta)/\lambda_1(\beta)]^r$. Thus, at β_c a nonanalytic behavior developes in this limit. The jump occurring in $\rho_2(\beta)/\lambda_1(\beta)$ implies that the decay of the correlations and the finite size corrections is qualitatively different in the Kac model depending on the sign of $\beta - \beta_c$. The decay is monotonic for $\beta > \beta_c$ and is oscillating with an alternating sign for $\beta < \beta_c$.

Finally, we discuss briefly properties of the spectrum of the generalized Kac models. In the field-free version of the complex case, the eigenfunctions are either symmetric or antisymmetric under the reflection $(z_1, z_2) \to (-z_1, -z_2)$. Indeed, the case $\beta = 0$ shows that the highest positive eigenvalue has an even eigenfunction, whereas the second highest eigenvalue, which is degenerate in modulus, has antisymmetric eigenfunctions. This follows from the fact that with ρ also the complex conjugate ρ^* is an eigenvalue of $\mathcal{L}$: if $g(z_1, z_2)$ is the eigenfunction to ρ then $g^*(z_1, z_2) \equiv [g(z_1^*, z_2^*)]^*$ is the eigenfunction to ρ^*. For β near zero the second highest eigenvalue is certainly complex and hence degenerate in absolute value. We do not know if for some real β the pair of eigenvalues reaches the real line. In this case the second highest eigenvalue would be degenerate. Contrary to the case of real λ the spectrum of the transfer operator for complex λ is hence not real for all real temperatures β.

Although even and odd functions do not form an invariant subspace in the presence of a magnetic field, our numerical investigations prove that the jump in ρ_2 at some negative temperature persists until the value of h or $|\lambda|$ becomes of order unity. We note that the phenomenon of level crossing is also present among the moduli of higher order eigenvalues in all versions of the Kac model.

It is worth mentioning that for the purpose of investigating a broad range of eigenvalues, the zeta function formalism [16,55,56] provides a technically more powerful framework than the iterative approach. By an appropriate tail resummation, the convergence can be made even faster than exponential. This method, however, does not yield any information concerning the eigenfunctions which are essential for characterizing the microscopic spin configurations.

VII. ASSOCIATED ONE-DIMENSIONAL MAPS

The thermodynamical formalism of one-dimensional (1D) maps with chaotic invariant sets defines quantities [3,9] which are the analogs of thermodynamical potentials expressed in terms of the map's properties. It implies that there exists an associated spin system the thermodynamics of which is governed by the same potential. The way to find a spin system for a given dynamics has extensively been studied [31–38]. Here we follow the opposite way and ask how a map with the same thermodynamics as a given spin system can be constructed. Even for Ising type spin chains there seem to exist several possibilities for this construction. In order to be specific, we restrict our attention to a class of 1D maps $f(x)$ which is topologically similar to (but more general than) the Bernoulli shift. The following properties are assumed:

(i) f maps the unit interval $I = [0, 1]$ onto itself or partially outside I;

(ii) The origin and the unity are two fixed points of the map f;

(iii) f possesses two inverse branches denoted by F_ϵ, $\epsilon = 0, 1$:

$$f(F_\epsilon(y)) = y \quad \text{and} \quad F_\epsilon(f(x)) = x. \tag{31}$$

The F_ϵ's are called the presentation functions [28]. They are assumed to be defined on the entire unit interval. This ensures that the dynamics of the map can be symbolically described by a complete set of binary codes and corresponds to the appearance of all binary microstates in an Ising type chain. We use the convention that $\epsilon = 0$ marks the inverse of the left branch of f.

In the thermodynamical formalism of dynamical systems the free energy $F(\beta)$ of a 1D map is defined via the partition sum [9]

$$\sum_{\{\epsilon\}} \exp\left[\beta \ln l(\epsilon_1 \dots \epsilon_n)\right] \sim \mathrm{e}^{-\beta F(\beta) n}, \quad n \gg 1, \tag{32}$$

where $l(\epsilon_1 \dots \epsilon_n)$ denotes the length of the cylinder $I_n(\epsilon_1 \dots \epsilon_n)$ labeled by the symbolic code $(\epsilon_1 \dots \epsilon_n)$. The set of the cylinders $I_n(\epsilon_1 \dots \epsilon_n)$ is nothing but the set of all the 2^n nth preimages of the unit interval. According to the standard notation [23], the symbolic code ϵ takes on 0 or 1 depending on whether the presentation function F_0 or F_1 is taken in the construction of the preimages, i.e., the cylinders are labeled according to the rule

$$(F_{\epsilon_1} \circ F_{\epsilon_2} \circ \cdots \circ F_{\epsilon_n})(I) = I_n(\epsilon_1 \epsilon_2 \dots \epsilon_n). \tag{33}$$

This means that the first code ϵ_1 specifies whether the cylinder lies below the left (0) or the right (1) branch of the map. Similarly, code ϵ_j provides the same information concerning the jth image of the cylinder under f.

First, we study the general question of how one can find a map associated with a binary spin chain with arbitrary two-body interactions. The Hamiltonian of the system of length n can then be written as

$$H = nE_0 - h \sum_{i=1}^{n} \sigma_i + \sum_{i=1}^{n-1} \sum_{k=1}^{n-i} V(\sigma_i, \sigma_{i+k}), \tag{34}$$

where V is the interaction energy between two spins σ_i and σ_{i+k} and h stands for a homogenous external magnetic field. Note that for later reference we introduced an energy constant E_0. Its value is completely irrelevant for measurable thermodynamical quantities but is, as we shall see, essential in the construction of the associated map.

In order to find such a map one has to define a one-to-one correspondence between the sets $\{\sigma_i\}_n$ and $\{\epsilon_i\}_n$ of spin configurations and symbolic codes. We have chosen the form [32]

$$\sigma_{n+1-i} = 1 - 2\epsilon_i, \quad i = 1, 2, \dots, n. \tag{35}$$

This implies that spin state $+1$ (-1) corresponds to code 0 (1).

Knowing the one-to-one correspondence between microstates and symbolic codes, one can identify the Boltzmann factors appearing in the partition sum of the map [Eq. (32)] and of the spin system described by Eq. (34). This leads to the relation

$$\ln l(\epsilon_1 \dots \epsilon_n) = -nE_0 + h\sum_{i=1}^{n}\sigma_i - \sum_{i=1}^{n-1}\sum_{k=1}^{n-i} V(\sigma_i, \sigma_{i+k}). \tag{36}$$

Here $(\epsilon_1 \dots \epsilon_n)$ denotes that symbolic code which uniquely corresponds to the spin configuration $(\sigma_1, \dots, \sigma_n)$.

The next step in the construction is to write down Eq. (36) taken at $n+1$. Because we have defined the order in which the symbols appear according to Eq. (33), we can write

$$\ln l(\epsilon_0\epsilon_1 \dots \epsilon_n) = -(n+1)E_0 + h\sum_{i=1}^{n+1}\sigma_i - \sum_{i=1}^{n}\sum_{k=1}^{n-i+1} V(\sigma_i, \sigma_{i+k}), \tag{37}$$

where $\epsilon_0 \in \{0,1\}$ is the new symbol corresponding to the last spin σ_{n+1}. By taking the difference between Eq. (37) and Eq. (36), we obtain

$$\ln \frac{l(\epsilon_0\epsilon_1 \dots \epsilon_n)}{l(\epsilon_1 \dots \epsilon_n)} = -E_0 + \sigma_{n+1}h - \sum_{i=1}^{n} V(\sigma_i, \sigma_{n+1}). \tag{38}$$

Note that the left-hand side of Eq. (38) is just the logarithm of the "daughter-to-mother" ratio [28] playing an important role in the theory of 1D maps. For $n \gg 1$ this ratio can be approximated by the derivative of the inverse map taken at some arbitrarily chosen point inside the cylinder $I_n(\epsilon_1 \dots \epsilon_n)$. This implies that we approximate the map on the cylinder sets I_n with straight lines which is a legitimate approximation for large n. Consequently, one can write

$$F'_\epsilon = \exp\left[-E_0 + (1-2\epsilon)h - u_\epsilon(y)\right], \tag{39}$$

where $\epsilon = 0, 1$ and y is an arbitrary chosen point within the cylinder $I_n(\epsilon_1 \dots \epsilon_n)$. The quantity

$$u_{0(1)}(y) = \lim_{n\to\infty}\sum_{i=1}^{n} V[\sigma_i, \sigma_{n+1} = 1(-1)] \tag{40}$$

gives the interaction energy of the last spin with a given configuration of the semi-infinite chain expressed as a function of position y of the cylinder $I_\infty(\{\epsilon_i\})$ rather than of the corresponding spin configuration $\{\sigma_i\}$. These functions will be called the *symbolic interaction functions* and are easy to construct numerically.

It has to be emphasized that Eq. (39) determines the presentation functions in terms of the location y of the cylinders. Unfortunately, it is not known *a priori* what the y's are. If the cylinders were all of equal length, y would be just $\hat{y} \equiv \sum_{i=1}\epsilon_i 2^{-i}$, i.e., the binary number representation of the symbolic code $\{\epsilon_i\}$ on the unit interval. Since this is in general not the case, we apply a self-consistent procedure to determine the presentation functions explicitly. As a first approximation, we assume that the cylinders of level n are all of equal length. The presentation functions $F_\epsilon^{(0)}$ are then constructed as continuous piecewise linear functions on these cylinders the slopes of which are given by (39). Next, we redefine the cylinder set by taking subsequent images of the unit interval with respect to these presentation functions. By iterating this procedure, one obtains a series of presentation functions $F_\epsilon^{(1)}$, $F_\epsilon^{(2)}, \dots$ which converge to a limit $F_\epsilon(y)$ and the corresponding partition tends to the generating partition taken with respect to the limiting functions. A sufficient condition of convergence is that the presentation functions have to be contracting, i.e., $|F'_\epsilon| < 1$ for any y. The essence of this procedure can best be illustrated by the example of a piecewise linear map corresponding to an Ising chain with nearest-neighbor interaction which is given in Appendix C.

Equation (39) defines the associated map f in terms of the magnetic field, energy constant, and the symbolic interaction functions. Note that the latter are independent of h. Equation (39) also shows how the energy constant influences the form of the presentation function. The role of E_0 is so essential, as we shall see below, that an associated map can only be found if it is greater than a critical value E_0^{**}.

VIII. SELF-SIMILARITY PROPERTIES AND THE DEPENDENCE ON THE ENERGY CONSTANT

Let us turn now to the particular case of the Kac model. We write down the formulas for the complex case which immediately turn into the results valid in the real case in the limit $\lambda_{\rm im} \to 0$. The interaction energy of two spins σ_i, σ_j is $-\sigma_i\sigma_j\lambda^{|j-i|}$ plus complex conjugate, therefore, the symbolic interaction function takes the form

$$u_\epsilon(y) = (-1)^\epsilon \tfrac{1}{2}\lim_{n\to\infty}\sum_{i=1}^{n}\sigma_{n+1-i}(\lambda^i + \lambda^{*i}). \tag{41}$$

By expressing the spin variables through the symbolic codes via Eq. (35), we obtain

$$u_\epsilon(y) = (-1)^\epsilon\left[\frac{\lambda}{1-\lambda} - \lim_{n\to\infty}\sum_{i=1}^{n}\epsilon_i(\lambda^i + \lambda^{*i})\right]. \tag{42}$$

We recall that variable y is the position of the cylinder $I_\infty(\{\epsilon_i\})$ that has to be determined by means of the self-consistent procedure described in the preceding section.

Before performing this computation it is worth plotting the symbolic interaction functions as functions of $\hat{y}$, the binary number representation of $\{\epsilon_i\}$. Finite approximants to $u_\epsilon(\hat{y})$ have been determined numerically and the results are exhibited in Fig. 8 for a few values of λ.

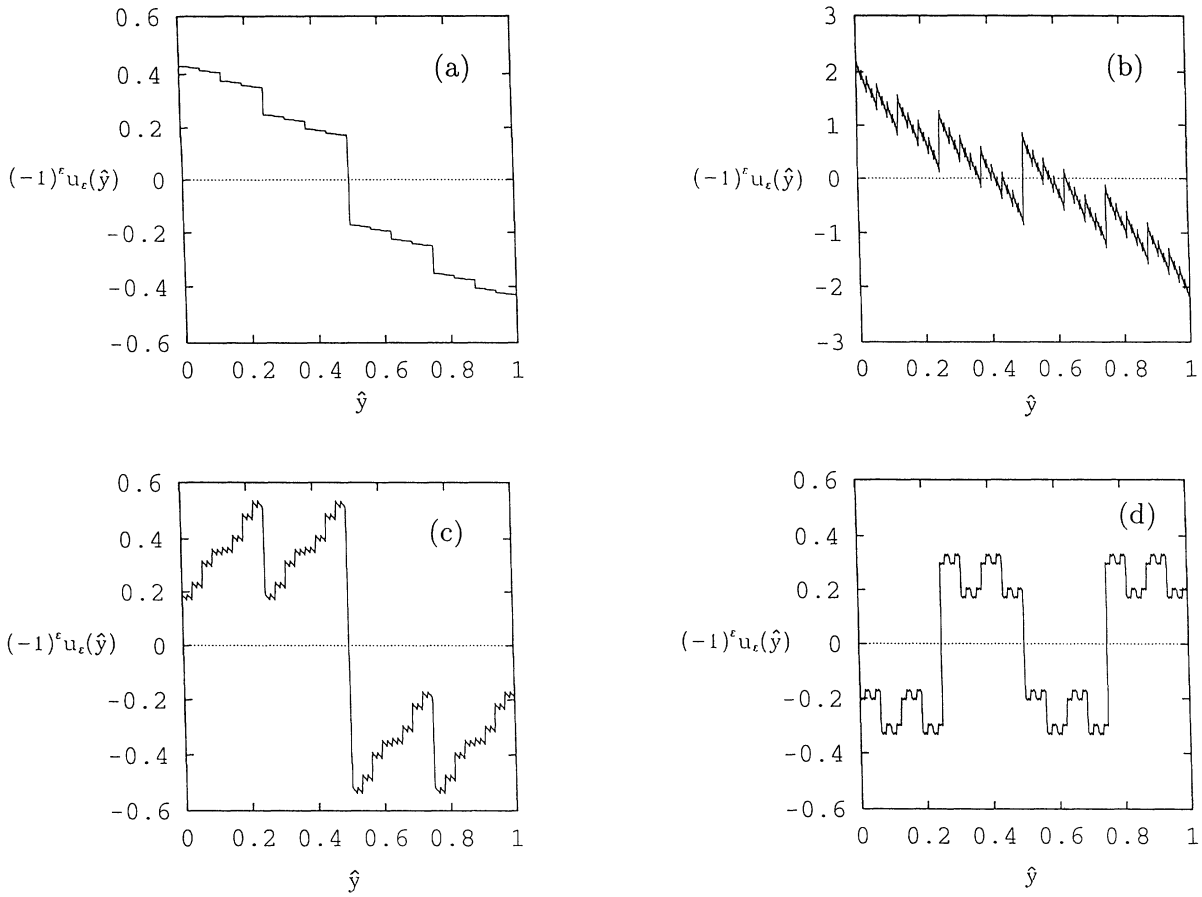

FIG. 8. Symbolic interaction functions $u_0(\hat{y}) = -u_1(\hat{y})$ plotted at (a) $\lambda = 0.3$, (b) $\lambda = 0.7$, and at $|\lambda| = 0.5$ with (c) $\varphi = \pi/2$ and (d) $\varphi = \pi/4$. These plots were obtained by dividing the $\hat{y}$ axis into equal boxes of size 2^{-n} with $n = 10$ and plotting the right-hand side of Eq. (42) vs $\hat{y} = \sum_{i=1} \epsilon_i 2^{-i}$.

Note the apparent fractal features.

A few remarks are in order. The codes ϵ_i and the spin variables ξ_i introduced in Sec. III are in one-to-one correspondence. Therefore, the symbolic interaction function yields essentially the relation between the spin configuration $\underline{\xi}$ and the variable x defined by Eq. (9) or $z_1 + z_2$ where z_i has been given by Eq. (13). Figure 8 clearly shows that in the real case the relation between $\underline{\xi}$ and x is one-to-one for $\lambda < 1/2$ only. This is reflected by the fact that $u_\epsilon(\hat{y})$ is the inverse of a devil's staircase function as long as $\lambda < 1/2$, and becomes a Weierstrass-like function for $\lambda > 1/2$ [57]. [At the borderline situation $\lambda = 1/2$ the graph of $u_\epsilon(\hat{y})$ is just a straight line.] It is interesting to note that the same functions also appear in the context of a Brownian diffusion problem [59].

The interaction parameter uniquely determines the fractal properties of the symbolic interaction function. This can best be seen in the real case. The symbolic interaction function is self-affine [58] for any real λ, i.e., has the generalized homogeneity property

$$u_\epsilon(\hat{y}) = a^{-H} u_\epsilon(a\hat{y}), \tag{43}$$

where H is called the roughness exponent [58]. It is easy to check that the symbolic interaction function is invariant under contracting the range of the $\hat{y}$ by 1/2 and simultaneously rescaling the variable u_ϵ by a factor of λ. Thus $a = 1/2$ and for the roughness exponent we obtain

$$H = \frac{\ln 1/\lambda}{\ln 2}. \tag{44}$$

The values where the plateaus of $u_\epsilon(\hat{y})$ are located for $\lambda < 1/2$ are just the points of the invariant set of the piecewise linear map $f(x) = x/\lambda - \sigma$ the inverse of which appears in operator (11). The invariant set of this map is a Cantor set of the fractal dimension

$$D_0 = \frac{\ln 2}{\ln (1/\lambda)} < 1. \tag{45}$$

For $\lambda > 1/2$ the graph of $u_\epsilon(\hat{y})$ is similar to that of a Weierstrass function. A scaling argument applied to the graph of $u_\epsilon(\hat{y})$ yields for its fractal dimension [57,58]

$$D_0 = 2 - H. \tag{46}$$

Since the values the function $u_\epsilon(\hat{y})$ and $u_\epsilon(y)$ can take on are the same as they depend on the code only, these results also imply that the original symbolic interaction functions $u_\epsilon(y)$ have fractal properties. In view of a previous comment, they also characterize the complex nature of the relation between spin configurations $\underline{\xi}$ and

the variable x appearing in the transfer operator.

We are now in a position to discuss the form of the associated maps and their free energies. Since the qualitative results are the same, in what follows we do not treat the cases of real and complex interaction parameter separately.

By combining Eq. (39) and Eq. (42), and using the self-consistent procedure for determining the cylinder position y, the presentation functions associated with the Kac model can be determined for every energy constant E_0. The free energy of the map will thus be $F(\beta) = \mathcal{F}(\beta) + E_0$ where $\mathcal{F}$ stands for the free energy computed with $E_0 = 0$ in Sec. IV. The quantity $\beta F(\beta)$, which is just the negative of the topological pressure of the map [9], differs from $\beta\mathcal{F}(\beta)$ in a linear term βE_0. By taking larger and larger positive values of E_0, the shape of the curve $\beta F(\beta)$ is changing mainly because of the increase in the slope of the right asymptote. It is only at sufficently large values of E_0 that this slope becomes positive. The graph of $\beta F(\beta)$ can only in such a case be similar to the one known for dynamical systems [9,25] which intersects the β axis at some positive value corresponding to the fractal (Hausdorff) dimension of the chaotic set (see Fig. 9).

It is worth emphasizing that there is *one single value* E_0^* of the energy constant which corresponds to a map exhibiting permanent chaotic behavior. This is the case (sometimes called fully developed chaotic map) when the unit interval I is mapped under f exactly two-to-one onto itself and when I is the attractor of the dynamics. The dimension is then unity and, therefore, $F(\beta)$ must vanish at $\beta = 1$ from which one finds the critical value $E_0 = E_0^*$ as $E_0^* = -\mathcal{F}(1)$ [for the corresponding presentation functions see Fig. 10(a)].

For E_0 greater than E_0^* the free energy $F(\beta)$ vanishes at some positive $\beta_0 < 1$, and the fractal dimension of the chaotic set is less than unity. The corresponding map

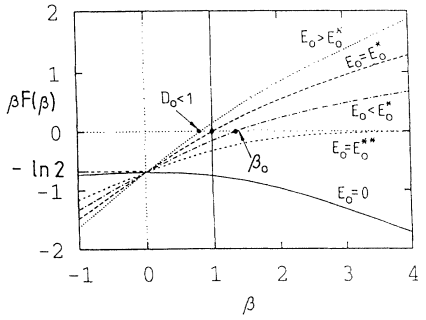

FIG. 9. The free energy of maps associated with the Kac model at different energy constants E_0 ($\lambda = 0.3$, $h = 0$). The energy constant $E_0^* = 0.753...$ corresponds to a fully developed chaotic map (heavy dashed line). Maps with $E_0 > E_0^*$ have fractal invariant sets with $D_0 < 1$. The free energy corresponding to $E_0 = 0.8$ has been plotted as a dotted line. For $E_0^{**} < E_0 < E_0^*$ the presentation functions overlap and a dynamics can only be defined in a random sense. The free energy plotted for $E_0 = 0.6$ (dashed dotted line) clearly shows that the intersection with the horizontal axis lies then at a value larger than one. For $E_0 < E_0^{**} = \lambda/(1-\lambda) = 3/7$ no associated map exists. Thus the free energy with $E_0 = 0$ (full line) can never appear in a chaotic context.

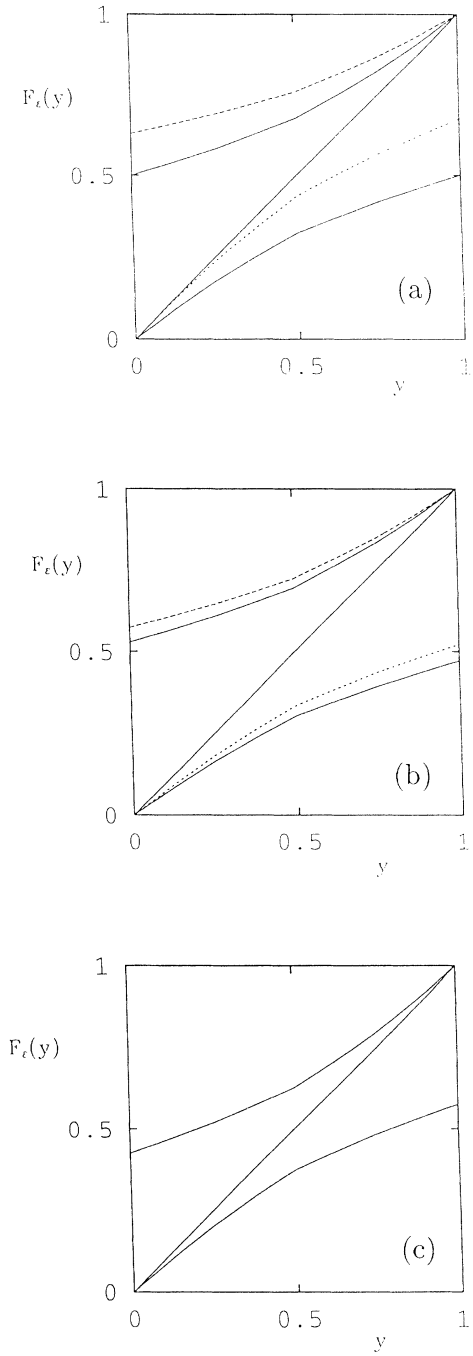

FIG. 10. Presentation functions corresponding to the Kac model at different E_0 values for $\lambda = 0.3$ obtained by constructing the symbolic interaction functions up to level $n = 10$. (a) Fully developed chaotic map, $E_0 = 0.753... = E_0^*$, (b) map with a gap, $E_0 = 0.8 > E_0$, and (c) map with overlapping branches, $E_0 = 0.6 < E_0$. Dashed lines in the first two cases show the effect of a magnetic field $h = 0.3$. Note that although the presentation functions are not smoothly differentiable because of the fractal nature of the symbolic interaction functions, in these figures they appear to be smooth. This is due to the fact that the jumps in u_ϵ are rather small as compared to the energy constant E_0 [see Eq. (39)]. In the limit $E_0 \to E_0^{**}$ both presentation functions would approach for $h = 0$ the diagonal. For $E_0 < E_0^{**}$ no associated map exists.

then possesses a gap and generates transient chaos [60]. The escape rate κ from the chaotic repeller underlying such a dynamics is just $F(1)$ from which $\kappa = E_0 + \mathcal{F}(1)$ follows. This means that increasing E_0 beyond E_0^* leads to maps with increasing escape rates (shorter chaotic lifetimes) and Lyapunov exponents, and with decreasing fractal dimensions [see Fig. 10(b)].

If E_0 becomes less than E_0^*, the presentation functions start to overlap [Fig. 10(c)]. One cannot speak any longer about a map f since the dynamics is not unique in the range of overlap. Nevertheless, the presentation functions are still well defined. One can also introduce a random dynamics by taking the branches of F_0 and F_1 with certain probabilities p and $1-p$. This random map has a strange attractor which is covered by the cylinders constructed via Eq. (36) [61,62]. The free energy $F(\beta)$ built up on the basis of these cylinders does not depend on the choice of the probability p and vanishes at some $\beta_0 > 1$. By further decreasing E_0 one reaches a value E_0^{**} when β_0 becomes infinite. If no magnetic field is present in the Kac model, this value is found to be $E_0^{**} = \lambda/(1-\lambda)$ which is just (-1) times the slope of the right asymptote to $\beta\mathcal{F}(\beta)$. As a consequence, the derivative of the presentation functions becomes then unity at both fixed points and the random dynamics is then intermittent [62]. The corresponding $\beta F(\beta)$ curve approaches the horizontal axis from below as $\beta \to \infty$ as shown in Fig. 9. Below E_0^{**} one cannot find any meaningfully defined map associated with the Kac model.

To check if the pictures provided by the transfer operator Eq. (1) and the Frobenius-Perron (FP) operator Eq. (2) are consistent, we studied the FP operator acting on the map associated with the Kac model, i.e., with presentation functions defined via Eqs. (39) and (42) shown in Fig. 10. We found that the free energy computed as the logarithm of the largest eigenvalue times (-1) of these maps was the same as that of the Kac model up to the additive constant E_0. Thus we numerically showed that Eqs. (1) and (2) have equivalent largest eigenvalues provided the presentation functions are chosen as described above.

IX. CONCLUDING REMARKS

The treatment of the Kac model by means of methods known from the theory of dynamical systems became possible because a representation of the transfer operator was found on simple function spaces. An analogous procedure has been worked out [50] for spin chains with interactions decaying faster than exponentially or with an exponential decay but multiplied with a polynomial expression of the distance. The case of an exponential decay divided by a polynomial of the distance would be of primary interest since it contains the case of polynomial interactions in the limit when the exponential decay tends to zero. Then a phase transition occurs provided the interaction decays slower than the second power of the distance [47]. Unfortunately, in such cases a simple functional representation of the transfer operator and the correct functions it has to act on has not been found yet. The situation as described in [50] seems to be quite similar to the problem one encounters in the discussion of the Frobenius-Perron operator for maps with neutral fixed points, where the good function spaces are also not known. Perhaps there is an intimate connection between these two problems.

Next, let us address the following question: what properties must a spin system have in order to lead to a smooth map of the interval? We emphasize that the map associated with the Kac model turned out to be not smoothly differentiable. It seems that spin chains with smoothly varying two-body interaction are always associated with such types of maps. In order to end up with an associated smooth map one thus has to include spin models with different types of multispin interactions. We believe that the smoothness of the associated map is a very special property and maps with fractal features will be found in most cases.

It is worth mentioning that the most general form of the Frobenius-Perron operator associated with a map $f(x)$ is of the form [3]

$$H_\phi \psi(x) = \sum_{\epsilon=0,1} e^{-\beta\phi_\epsilon(x)} \psi(f_\epsilon^{-1}(x)), \tag{47}$$

where $\phi_\epsilon(x)$ can be a general function, and $f_\epsilon^{-1}(x)$ denotes the two inverse branches of the map. Comparing this with Eqs. (1) and (11) we immediately see that with the choice

$$\phi_\epsilon(x) = -(1-2\epsilon)(Jx+h), \tag{48}$$

H_ϕ is exactly the same as $\mathcal{L}$ provided the map is defined by the presentation functions $\lambda(1-2\epsilon+y)$. With this choice of ϕ_ϵ, the map associated with the Kac model is a piecewise linear one. The smoothness of the associated maps thus also depends on ϕ but seems to be an exceptional property in the space of ϕ functions, too. The choice we investigated corresponds to $\phi_\epsilon(x) = -\ln|F_\epsilon'(x)|$, which leads to Eq. (2). This is a natural choice in the theory of dynamical systems and has intensively been studied. The famous relation $F(D_0) = 0$, for example, only holds with this choice of ϕ. According to a recent finding [56] one can always construct a $\phi(x)$ for any given spin chain so that the associated map is smooth but eventually higher dimensional. In view of this observation it would be interesting looking for two- and higher-dimensional dynamical systems associated with the Kac model.

ACKNOWLEDGMENTS

The authors are indebted to C. Beck, P. Cvitanović, F. Iglói, I. Kondor, P. Szépfalusy, G. Vattay, and J. Vollmer for useful discussions. This work was partially supported by the Hungarian Science Foundation under Grant Nos. OTKA 2090 and OTKA T4439, by the International Relation Offices of Hungary and Germany, Project X231.3, and by the Foundation for Hungarian Higher Education and Research.

APPENDIX A: PROPERTIES OF THE ODD EIGENFUNCTION BELOW β_c

In this appendix we show that the eigenfunction g_2 belonging to the largest eigenvalue ρ_2 in the class of odd functions has infinitely many nodes below β_c. Let $x^* \geq 0$ be a node of $g_2(x)$ whose eigenvalue equation is given by

$$e^{\beta x} g_2(\lambda + \lambda x) + e^{-\beta x} g_2(-\lambda + \lambda x) = \rho_2(\beta) g_2(x). \quad \text{(A1)}$$

Let us now choose the value of x so that

$$-\lambda + \lambda x = x^*. \quad \text{(A2)}$$

Inserting (A2) in (A1) results in

$$e^{\beta(1+x^*/\lambda)} g_2(2\lambda + x^*) = \rho_2(\beta) g_2(1 + x^*/\lambda). \quad \text{(A3)}$$

Since for $\beta < \beta_c$ the eigenvalue $\rho_2(\beta)$ is negative, from this relation and from the continuity of g_2 we conclude that another node x_1^* must exist in the interval

$$2\lambda + x^* < x_1^* < 1 + x^*/\lambda, \quad \text{(A4)}$$

or

$$1 + x^*/\lambda < x_1^* < 2\lambda + x^* \quad \text{(A5)}$$

depending on whether $x^* > 2\lambda(\lambda - 1/2)/(1 - \lambda)$ or not. Therefore, any node x^* of g_2 determines *another* one $x_1^* > x^*$ for $\beta < \beta_c$. By taking the origin as the first node $x_0^* = 0$, the next one x_1^* is found to lie in the range $(2\lambda, 1)$ if $0 < \lambda < 1/2$ and in the range $(1, 2\lambda)$ if $1/2 < \lambda < 1$. In an analogous way, x_1^* determines $x_2^*, \ldots$, and so on. If n is large enough, Eq. (A4) holds and one has

$$2\lambda + x_n^* < x_{n+1}^* < 1 + x_n^*/\lambda. \quad \text{(A6)}$$

Numerical evidence shows that x_{n+1}^* is very close to the upper bound, i.e., $x_{n+1}^* \approx 1 + x_n^*/\lambda$. This yields for x_n^* a geometrical series: $x_{n+1}^* \approx x_n^*/\lambda$ with ratio $1/\lambda > 1$.

APPENDIX B: COMPUTATION OF CROSSING EIGENVALUES

Here we present a numerical method allowing us to compute the two eigenvalue branches ρ_2 and ρ_4 around their intersection point β_c. Let us perform the computation for the quantity (21) for levels $n-1$, n, and $n+1$, respectively, and introduce the notation

$$c_i \equiv \frac{\mathcal{L}^{n+i} g_0(x)}{\mathcal{L}^{n+i-1} g_0(x)}, \quad i = 0, 1, 2. \quad \text{(B1)}$$

Assuming that eigenvalues ρ_2 and ρ_4 cross each other at β_c, we can approximate $\mathcal{L}^n g_0(x)$ by the first two terms of Eq. (25) for $n \gg 1$:

$$\mathcal{L}^n g_0(x) \simeq \rho_2^n A(x) + \rho_4^n B(x). \quad \text{(B2)}$$

Then we get for c_i

$$c_i \simeq \rho_2 \frac{1 + X^{n+i} C(x)}{1 + X^{n+i-1} C(x)}, \quad \text{(B3)}$$

where the abbreviations

$$X \equiv \frac{\rho_4}{\rho_2} \quad \text{(B4)}$$

and $C(x) \equiv A(x)/B(x)$ have been used. Eliminating the function $C(x)$ from (B3) taken at $i = 0$ and 1 we get

$$\frac{c_0 - \rho_2}{\rho_2 X - c_0} = \frac{c_1 - \rho_2}{\rho_2 X^2 - c_1 X}, \quad \text{(B5)}$$

and at $i = 1$ and 2 we get

$$\frac{c_1 - \rho_2}{\rho_2 X - c_1} = \frac{c_2 - \rho_2}{\rho_2 X^2 - c_2 X}. \quad \text{(B6)}$$

Finally, these equations yield for ρ_2

$$\rho_2^2(c_1 - c_0) + \rho_2 c_1(c_0 - c_2) + c_0 c_1(c_2 - c_1) = 0, \quad \text{(B7)}$$

with solutions $\rho_2^{\pm}$. Using the Viète formulas and (B4)–(B6) the properties

$$\rho_2^+ = \rho_4^- \quad \text{and} \quad \rho_2^- = \rho_4^+ \quad \text{(B8)}$$

follow. Thus measuring the quantities c_0, c_1, and c_2 we can compute both ρ_2 and ρ_4 as the solutions of (B7). This method seems to be very powerful, because for $n = 9$ we get ρ_2 and ρ_4 even around β_c with a precision up to 8–9 digits which is impossible from Eqs. (21) and (26). We observed that for even values of n the quantities c_0 and c_2 go to infinity while c_1 tends to zero when β approaches β_c which supports the fact that $\rho_2 = -\rho_4$ and $A(x) \equiv B(x)$ at β_c. Equation (B8) also shows that ρ_4 for $\beta < \beta_c$ is the analytical continuation of ρ_2 from $\beta > \beta_c$, and vice versa, as mentioned before.

APPENDIX C: PRESENTATION FUNCTIONS FOR THE ISING MODEL

The interaction energy in an Ising chain is given as

$$V(\sigma_i, \sigma_{i+1}) = -J\sigma_i\sigma_{i+1}. \quad \text{(C1)}$$

Thus the symbolic interaction is of the form

$$u_\epsilon(y) = (-1)^{\epsilon+1} \lim_{n\to\infty} J\sigma_n. \quad \text{(C2)}$$

It can take two values only: $+J$ and $-J$. Equation (39) then implies that the slope of the presentation functions can be one of the four values $\exp[-E_0 + (1 - 2\epsilon)h \pm J]$. The sign of J depends on the first code ϵ_1 of the cylinders. It has to be positive if $\epsilon_1 = 0$ on the lower branch ($\epsilon = 0$) or $\epsilon_1 = 1$ on the upper branch ($\epsilon = 1$). One has to determine where the division points between these segments lie. We use arbitrary division points $y_0^{(0)}$, $y_1^{(0)}$. The approximate presentation functions $F_0^{(0)}$ and $F_1^{(0)}$ are first constructed on the intervals $[0, y_0^{(0)}]$ and $[y_1^{(0)}, 1]$, respectively, with slopes $a_1^{-1} = \exp(-E_0 + h + J)$ and $a_4^{-1} = \exp(-E_0 - h + J)$. Then we add two new

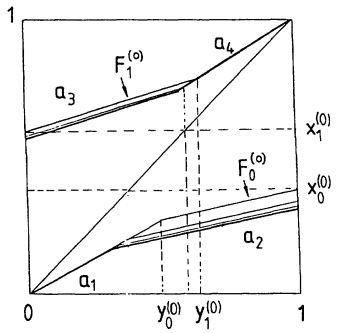

FIG. 11. Iteration procedure $F_\epsilon^{(0)}, F_\epsilon^{(1)}, \ldots$, to construct the presentation function for the Ising model. The heavy line obtained in the limit of infinite iterations represents the exact presentation functions F_0, F_1. The inverse slopes of the presentation functions' branches are denoted by $a_1, \ldots, a_4$. Arbitrary initial division points $y_0^{(0)}$ and $y_1^{(0)}$ were taken. The diagram shows that the convergence is exponentially fast. This also illustrates the method how the presentation functions were determined for the Kac model.

branches with slopes $a_2^{-1} = \exp(-E_0 + h - J)$ and $a_3^{-1} = \exp(-E_0 - h - J)$ so that the presentation functions $F_0^{(0)}$, $F_1^{(0)}$ are continuous in $y_0^{(0)}$ and $y_1^{(0)}$. This construction determines the end points $x_0^{(0)}$, $x_1^{(0)}$ uniquely (see Fig. 11). Next, we construct the new division points $y_{0,1}^{(1)}$ by taking the preimages of $x_0^{(0)}$ and $x_1^{(0)}$ with respect to branches 0 and 1, respectively. Consequently, the end points are also changed to some $x_0^{(1)}$ and $x_1^{(1)}$. By repeating the procedure we can show that the series of $y_0^{(n)}$ and $y_1^{(n)}$ belonging to the presentation functions $F_\epsilon^{(n)}$ are determined by the recursive formulas,

$$y_0^{(n+1)} = \frac{1}{a_2} + \left(\frac{1}{a_1} - \frac{1}{a_2}\right) y_0^{(n)} \tag{C3}$$

and

$$y_1^{(n+1)} = 1 - \frac{1}{a_3} - \left(\frac{1}{a_4} - \frac{1}{a_3}\right)(1 - y_1^{(n)}). \tag{C4}$$

Since all the slopes a_i are larger than 1, the iteration is *converging*, and the limiting values

$$y_0 = \frac{a_1}{a_1 a_2 + a_1 - a_2} \tag{C5}$$

and

$$y_1 = 1 - \frac{a_4}{a_4 a_3 + a_4 - a_3} \tag{C6}$$

are independent of the initial choice. This defines the exact presentation functions F_ϵ corresponding to the Ising chain at energy constant zero. They are piecewise linear functions containing two straight line segments. The break points are mapped exactly onto the end points [38]. This is nothing but the condition that the partition is a Markov partition.

[1] Y. G. Sinai, Russ. Math. Surveys **166**, 21 (1972).
[2] R. Bowen, Lect. Notes Math. **470**, 1 (1975).
[3] D. Ruelle, *Thermodynamic Formalism* (Addison-Wesley, Reading, 1978).
[4] G. Keller, Commun. Math. Phys. **96**, 181 (1984); D. Ruelle, Phys. Rev. Lett. **56**, 465 (1986); D. Ruelle, J. Stat. Phys. **44**, 281 (1986).
[5] P. Collet, J. Lebowitz, and A. Porzio, J. Stat. Phys. **47**, 609 (1987); A. Arneodo and M. Holschneider, *ibid.* **50**, 995 (1988); D. Bessis *et al.*, *ibid.* **51**, 109 (1988).
[6] V. Baladi, J. P. Eckmann, and D. Ruelle, Nonlinearity **2**, 119 (1989); A. O. Lopes, SIAM J. Math. Anal. **20**, 1243 (1989).
[7] M. J. Feigenbaum, M. H. Jensen, and I. Procaccia, Phys. Rev. Lett. **56**, 1503 (1986).
[8] M. H. Jensen, L. P. Kadanoff, and I. Procaccia, Phys. Rev. **A36**, 1409 (1987).
[9] T. Bohr and D. Rand, Physica D **25**, 387 (1987).
[10] M. J. Feigenbaum, J. Phys. **46**, 919 (1987); **46**, 925 (1987).
[11] M. Kohmoto, Phys. Rev. A **37**, 1345 (1987).
[12] P. Szépfalusy, T. Tél, A. Csordás, and Z. Kovács, Phys. Rev. A **36**, 3525 (1987).
[13] H. Mori *et al.*, Prog. Theor. Phys. **81**, 60 (1989).
[14] T. Kobayashi *et al.*, Prog. Theor. Phys. **82**, 1 (1989).
[15] R. Badii, Riv. Nuovo Cimento **12**, 1 (1989).
[16] R. Artuso, E. Aurell, and P. Cvitanović, Nonlinearity **3**, 325, 361 (1990).
[17] H. Fujisaka and H. Shibata, Prog. Theor. Phys. **85**, 187 (1991).
[18] C. Beck, Physica D **50**, 1 (1991).
[19] X. J. Wang, Phys. Rev. A **40**, 6647 (1989); H. Fujisaka and M. Inoue, Phys. Rev. A **41**, 5302 (1990); A. Porzio, J. Stat. Phys. **58**, 923 (1990).
[20] Z. Kovács and T. Tél, Phys. Rev. A **45**, 2270 (1992).
[21] R. Stoop *et al.*, Z. Naturforsch. **46a**, 642 (1991); R. Stoop and J. Parisi, Phys. Rev. A **43**, 1802 (1991); R. Stoop *et al.*, Physica D **50**, 405 (1991); R. Stoop, Phys. Rev. A **46**, 7450 (1992); Phys. Lett. A **173**, 369 (1993).
[22] H. Shigematsu, J. Stat. Phys. **66**, 727 (1992).
[23] C. Beck and F. Schlögl, *Thermodynamics of Chaotic Systems* (Cambridge University Press, Cambridge, 1993).
[24] P. Szépfalusy and T. Tél, Phys. Rev. A **34**, 2520 (1986).
[25] T. Tél, Phys. Rev. A **36**, 2507 (1987).
[26] H. Fujisaka and M. Inoue, Prog. Theor. Phys. **78**, 268 (1987).
[27] A. Csordás and P. Szépfalusy, Phys. Rev. A **38**, 2582 (1988).
[28] M. J. Feigenbaum, J. Phys. **52**, 527 (1988).
[29] M. J. Feigenbaum, I. Procaccia, and T. Tél, Phys. Rev. A **39**, 5359 (1989).
[30] T. Prellberg and J. Slawny, J. Stat. Phys. **60**, 503 (1992).
[31] D. Katzen and I. Procaccia, Phys. Rev. Lett. **58**, 169 (1987).

[32] M. H. Jensen and T. Bohr, Phys. Rev. A **36**, 4904 (1987).
[33] P. Gaspard and X. J. Wang, Proc. Natl. Acad. Sci. U.S.A. **85**, 4591 (1988).
[34] X. J. Wang, Phys. Rev. A **39**, 3214 (1989); Theor. Phys. **82**, 682 (1989).
[35] S. Sato and K. Honda, Phys. Rev. A **42**, 3233 (1990).
[36] K. Honda and H. Kodama, Phys. Lett. A **149**, 101 (1990).
[37] K. Honda, S. Sato, and H. Kodama, Phys. Rev. A **43**, 2669 (1991).
[38] P. Szépfalusy, T. Tél, and G. Vattay, Phys. Rev. A **43**, 681 (1991).
[39] M. Kac, Phys. Fluids **2**, 8 (1959); *Brandeis University Summer Institute in Theoretical Physics* (Gordon-Breach, New York, 1966), Vol. 1.
[40] G. A. Baker, Jr., Phys. Rev. **122**, 1477 (1961).
[41] M. Kac and E. Helfond, J. Math. Phys. **4**, 1078 (1963).
[42] M. Kac, G. E. Uhlenbeck, and P. C. Hemmer, J. Math. Phys. **4**, 216 (1963); J. Lebowitz and O. Penrose, *ibid.* **7**, 98 (1966).
[43] K. S. Viswanathan and D. H. Mayer, Physica A **89**, 97 (1977).
[44] A. Hucht, Physica A **183**, 223 (1992).
[45] L. Pietronero and S. Strässler, Phys. Rev. Lett. **42**, 188 (1979); T. Geszti, Phys. Rev. B **30**, 1811 (1984).
[46] P. Reichert and R. Schilling, Phys. Rev. B **32**, 5731 (1985); J. Vollmer, W. Breymann, and R. Schilling, Phys. Rev. B **47**, 11 767 (1993).
[47] C. J. Thompson, *Mathematical Statistical Mechanics* (Macmillan, New York, 1971); in *Phase Transitions and Critical Phenomena*, edited by C. Domb and M. Green (Academic, London, 1972), Vol. 1.
[48] C. Kittel, Solid State Phys. **22**, 1 (1968).
[49] G. Thoulouse, Commun. Phys. **2**, 115 (1977); J. Vannimenus and G. Thoulouse, J. Phys. C **10**, L537 (1977).
[50] D. H. Mayer, *The Ruelle-Araki Transfer Operator in Classical Statistical Mechanics*, Lecture Notes in Physics Vol. **123** (Springer-Verlag, Berlin, 1980).
[51] H. Kramers and G. Wannier, Phys. Rev. **68**, 252 (1941); E. W. Montall, J. Chem. Phys. **9**, 706 (1941); E. N. Lassette and J. P. Howe, *ibid.* **9**, 747 (1941); R. Kubo, Busseiron Kenkyu **1**, (1943); G. F. Newell and E. W. Montall, Rev. Mod. Phys. **25**, 353 (1953).
[52] D. H. Mayer, Lett. Math. Phys. **1**, 335 (1976).
[53] B. Moritz, Diploma work (in German), RWTH Aachen, 1989.
[54] M. N. Barber, in *Phase transitions and Critical Phenomena*, edited by C. Domb and J. L. Lebowitz (Academic, London, 1983), Vol. 8, p. 145.
[55] R. Mainieri, Ph.D. thesis, New York University, 1990; Phys. Rev. A **45**, 3580 (1992).
[56] R. Mainieri, Geometrization of Spin System Using Cycle Expansions, 1992 (unpublished).
[57] T. Tél, Z. Naturforsch. **43a**, 1154 (1988).
[58] A.-L. Barabási, P. Szépfalusy, and T. Vicsek, Physica A **178**, 17 (1991).
[59] C. Beck, Physica A **169**, 324 (1990).
[60] T. Tél, in *Directions in Chaos*, edited by Hao Bai-lin (World Scientific, Singapore, 1990), Vol. 3, pp. 149–211.
[61] G. Györgyi and P. Ruján, J. Phys. C **17**, 4207 (1984).
[62] C. Van den Broeck and T. Tél, in *From Phase Transitions to Chaos*, edited by G. Györgyi *et al.* (World Scientific, Singapore, 1992), pp. 227–236.